AIAA 2003-1546

Imparting Desired Attributes by Optimization in Structural Design

Jaroslaw Sobieszczanski-Sobieski (j.sobieski@larc.nasa.gov)
NASA Langley Research Center
MS 240, Hampton, VA 23681-2199

Gerhard Venter (gventer@vrand.com)
Vanderplaats Research and Development, Inc.
1767 S 8th Street, Suite 200, Colorado Springs, CO 80906

44th AIAA/ASME/ASCE/AHS Structures, Structural Dynamics, and Materials Conference
April 7-10, 2003
Norfolk, Virginia

Imparting Desired Attributes by Optimization in Structural Design

Jaroslaw Sobieszczanski-Sobieski (j.sobieski@larc.nasa.gov) *
NASA Langley Research Center
MS 240, Hampton, VA 23681-2199

Gerhard Venter (gventer@vrand.com) †
Vanderplaats Research and Development, Inc.
1767 S 8th Street, Suite 200, Colorado Springs, CO 80906

Commonly available optimization methods typically produce a single optimal design as a constrained minimum of a particular objective function. However, in engineering design practice it is quite often important to explore as much of the design space as possible with respect to many attributes to find out what behaviors are possible and not possible within the initially adopted design concept. The paper shows that the very simple method of the sum of objectives is useful for such exploration. By geometrical argument it is demonstrated that if every weighting coefficient is allowed to change its magnitude and its sign then the method returns a set of designs that are all feasible, diverse in their attributes, and include the Pareto and non-Pareto solutions, at least for convex cases. Numerical examples in the paper include a case of an aircraft wing structural box with thousands of degrees of freedom and constraints, and over 100 design variables, whose attributes are structural mass, volume, displacement, and frequency. The method is inherently suitable for parallel, coarse-grained implementation that enables exploration of the design space in the elapsed time of a single structural optimization.

Introduction

MOST structural optimization applications have minimum weight as the objective. However, the complete description of a structure entails many other quantities that the designer may wish to influence, especially in a multi-disciplinary environment in which these quantities couple the structure to other disciplines and subsystems. These quantities that collectively characterize the structure, will henceforth be referred to as the attributes.

This paper shows how multi-objective (Pareto) optimization enables a degree of control over the attributes in structural design. A body of literature exists on multi-objective optimization. However, its focus seems to be (e.g., Stadler[1]) on the perfor-

---

*Senior Research Scientist, Analytical and Computational Methods Branch, Structures and Materials Competency, AIAA Fellow
†Senior R&D Engineer, AIAA Member

mance and theoretical aspects of the methodology rather than on issues of a direct interest to the structural designer. The practitioner toolbox for multi-objective optimization contains several techniques that differ in terms of computational efficiency, effectiveness, and ease of use. The following are typical examples of these techniques:

1. Composite objective function $F = \sum_i w_i f_i$ where w_i is a weighting factor assigned to the objective component f_i

2. Discrepancy objective function $F = \sum_i \left(f_i - f_i^T\right)^2$ where f_i^T is a target set for the objective components f_i

3. Goal Programming (a.k.a. Compromise Programming) in which the objective function may be formulated as $F = \sum_i \left|f_i - f_i^T\right|$

4. Global optimization in which the objective

function is the same as in item 2 but the targets are derived by optimizing each objective separately, one at a time, i.e., $f_i^T = \min\left(f_i:\ X:\ g(X) \le 0\right)$, where f_i is the ith attribute

5. Normal constraint method (e.g., Ismail-Yahaya and Messac[2])

Among these techniques, the composite objective function technique appears by far the simplest to use. It is also a natural choice for coarse-grained parallel computing with existing analysis and optimization programs - an important advantage in view of the multiprocessor computers becoming commonly available. On the other hand, the method is not the mathematician's favorite because of its shortcomings examined in, for example, Ismail-Yahaya and Messac,[2] Messac and Ismail-Yahaya,[3] Das and Dennis,[4] Koski[5] and Belegundu and Chandrupatla.[6] The shortcomings pointed out most often are the method missing some of the Pareto-points and its inability to return points uniformly distributed over the Pareto-frontier (remedies were proposed, e.g., Ismail-Yahaya and Messac[2]).

However, these shortcomings are not decisive herein because the purpose of this paper is not to contribute to the theory of Pareto-optimization. Its intent is merely to establish a practical method for exploration of the design space simultaneously for many design attributes, including Pareto- and non-Pareto points alike, and to illustrate the method with an example of dimensionality large enough to be relevant to real-world applications. The remainder of the paper shows that, for the above purpose, the composite objective function appears to be a good choice.

Composite Objective Function Properties

It is useful to begin with preliminaries that usually appear in literature in a mathematical form but, for a difference, will be presented here with emphasis on descriptive geometry. Consider a convex design space (X_1, X_2) whose boundary is formed by constraints $c_1 = 0$ and $c_2 = 0$ as depicted in Fig. 1. Two linearly independent objective functions, f_1 and f_2, exist and are assumed, temporarily, to be linear. Then, their contours may be represented by two sets of straight lines as depicted in Fig. 1, and the arrows, G_1 and G_2, portray the gradient vectors of these functions. Monotonicity of linear functions determines that the constrained extrema of f_1 and f_2 lie at the points A, B, D, E, where the contour lines

are tangent to the constraint boundary curves, consistent with the nature of most engineering problems in which minima are, typically, constraint-bound as opposed to free minima located inside of the feasible space.
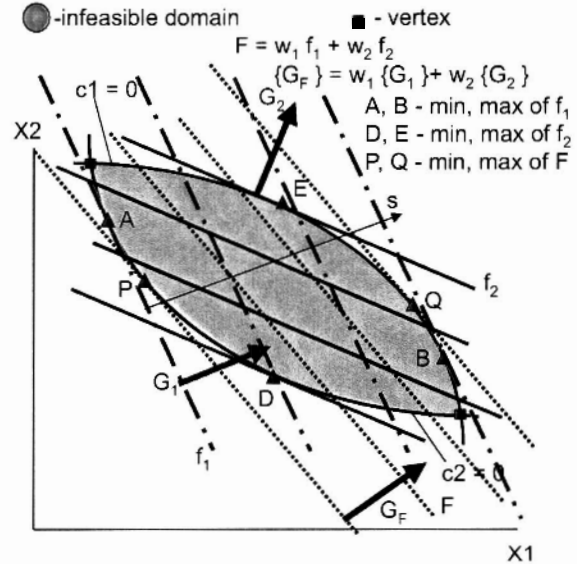

Fig. 1   Composite Objective Function

A composite objective

$$F = w_1 f_1 + w_2 f_2 \tag{1}$$

has contours shown in Fig. 1 by the third set of straight lines, its gradient vector

$$\boldsymbol{G_F} = w_1 \boldsymbol{G_1} + w_2 \boldsymbol{G_2} \tag{2}$$

and its extrema lie at the tangency points P and Q.

Turning to Fig. 2, the vectors $w_1 \boldsymbol{G_1}$ and $w_2 \boldsymbol{G_2}$ may be regarded as skew coordinates (the objective functions must be linearly independent to avoid the degenerate case of co-linear coordinate axes). Then, it is apparent that by choosing the signs and values of w_1 and w_2, one may orient $\boldsymbol{G_F}$ at any angle a in a full $0°$ to $360°$ range.
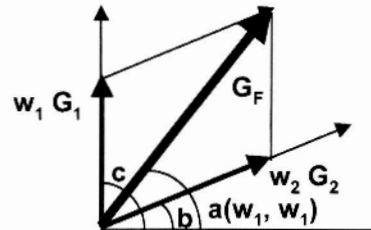

Fig. 2   Gradient Vector

One full rotation of $\boldsymbol{G_F}$ through $0°$ to $360°$ results in the extremum points P and Q tracing the entire

is present.

Based on the foregoing geometrical argument illustrated in Figs. 1–3, one may assert that optimization defined as

Given f_i, where $i = 1, ..., N_f$
          w_i, where $i = 1, ..., N_f$
          g_j, where $j = 1, ..., N_c$

Minimize $F = \sum_i w_i \ f_i$

Satisfy $g_j \leq 0$

when repeated for w_i taken in a sufficiently wide interval, returns design points located either on the feasible space boundary or inside of that space. The points returned include the Pareto- and non-Pareto points. In principle, to obtain the full coverage, the w_i intervals would have to be $(-\infty$ to $+\infty)$ so in practical applications the interval spans need to be set judgmentally.

The remainder of the paper presents numerical examples of using the above outlined optimization technique as a tool to explore multi-attribute design spaces.

Numerical Examples

Small scale, introductory example

The concept of controlling the object attributes by multi-objective optimization may be illustrated by the following example that is utterly simple and yet instructive. The example is a cantilever box-beam of length L with a rectangular, b-by-h, thin-walled cross-section, loaded by a force P at the tip, as depicted in Fig. 6.
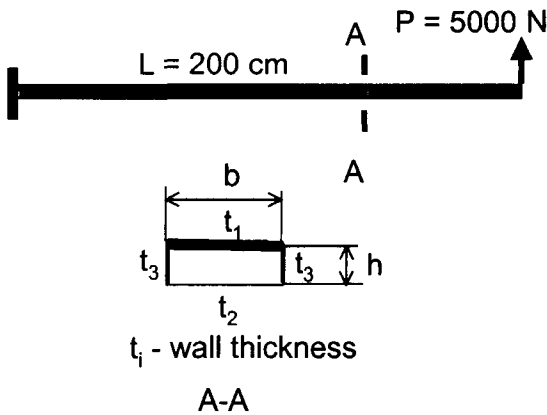

Fig. 6 Cantilever Beam Example

The multi-objective optimization problem is defined as

Given E - Young's modulus
          L - Beam Length
          σ_a - Allowable stress

Find $X = b, h, t_1, t_2, t_3$

Minimize $F = w_1 \frac{W}{W_0} + w_2 \frac{S}{S_0} + w_3 \frac{T}{T_0} + w_4 \frac{B}{B_0}$

Satisfy $g_j \leq 0$

where: W - structural weight (tantamount to the material volume); S - bending stiffness with respect to the tip load P; T - the lowest torsion mode frequency; B - the lowest bending mode frequency; g_j - constraints on normal stress, and on buckling of the top panel. The bending and torsional stiffnesses involved in the frequency calculations are expressed, respectively, by the strength of materials beam formulas and by the thin-walled box beam formulas due to Bredt. The numerical disparity of the terms in the above formulation was removed by the use of normalization with the initial values.

The solution obtained numerically (using the Microsoft Excel solver) for various values of w_i generates a family of the box-beam designs entailing a broad variety of the cross-sectional dimensions, as illustrated by a few examples in Fig. 7 for various w_1 and w_2. The w_i settings appear beneath cross-sections that are drawn to scale in regard to the b and h dimensions. The wall thicknesses and the attributes are inscribed and so are the attributes. The result sample continues in Table 1 that shows how some of the attributes change when $w_1 = constant$, $w_3 = 0$, and w_2 and w_4 vary. These results were selected from about 40 different Excel Solver executions.

Table 1 Cantilevered Beam Results

w_2	W/W_0	S/S_0	B/B_0	T/T_0
-1.0	4.4053	6.1347	0.1924	0.2934
-0.5	1.3265	1.9824	0.6167	1.0300
0.0	1.0000	1.0000	1.0000	1.0000
0.5	1.0496	0.7685	1.1135	0.6567
1.0	1.2471	0.4987	1.2680	0.6180
2.0	1.5202	0.3040	1.4711	0.6347
4.0	1.8531	0.1853	1.7067	0.6511
8.0	2.2590	0.1129	1.9800	0.6491
max/min	1.94	55.73	10.42	3.55

The last row of Table 1 shows the ratios of the maximum/minimum entries in each column. These ratios indicate that the attributes vary in quite a broad range as a function of w_2, for instance the ratio $\max(S/S_0)/\min(S/S_0) = 55.73$, while the ratio

closed circuit of the constraint boundary consisting of the contours $c_1 = 0$ and $c_2 = 0$. Each location of P in that travel corresponds to a pair of values of f_1 and f_2, and the same is true for Q. These values are bounded by the minimum and maximum of f_1 and f_2 marked by A, B, D, E. Hence, a plot of f_1 vs. f_2 may be constructed, corresponding to the full circuit travel of P and Q, as seen in Fig. 3, in which the Pareto-minimum segment extends from points 1 to 2, and the Pareto-maximum segment stretches from 3 to 4. The corresponding Pareto segments in Fig. 1 are A–D and B–E. The points not in these segments are non-Pareto.

pareto: minimum, maximum
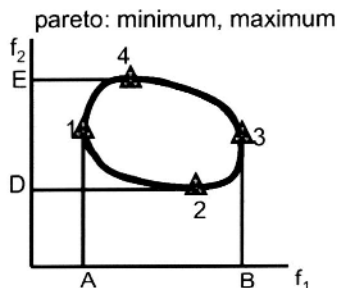
Fig. 3 f_1 **versus** f_2

The above vector geometry clearly shows that the normalization of the vector of w to $\sum_i w_i = 1$ that often appears in the weighted sum formulation used in Pareto-optimization, for example Eschenauer[7] and Koski,[5] restricts the attainable orientations of $\boldsymbol{G_F}$ to $b \le a \le c$ (see Fig. 2). This orientation restriction is immediately seen in a two-objectives case, in which normalized $F = 1f_1 + (1 - w)f_2$. Such an F formulation results in $w_1 \boldsymbol{G_1}$ whose sign in Fig. 2 may be positive or negative to be replaced with a positive only $1\boldsymbol{G_1}$ so that any $\boldsymbol{G_F}$ orientation below $w_2 \boldsymbol{G_2}$ is unattainable. Returning to Figs. 1 and 2, it is self-evident that optimization with the above normalized formulation is still adequate to identify the min/max Pareto-frontiers A–D and B–E but is not capable to discover the non-Pareto points.

Removal of the linearity assumption for f_1 and f_2 leaves the above argument qualitatively unchanged, even though the straight contours of f_1 and f_2 become curved. However, it introduces a possibility of the minimum of F leaving P and moving to M that falls in the feasible space as illustrated in Fig. 4 that shows f_1, f_2, and F plotted along direction marked s in Fig. 1. The reasoning based on the geometry presented in Figs.1–4 readily extends to higher dimensions in terms of the number of objectives f and design variables x.

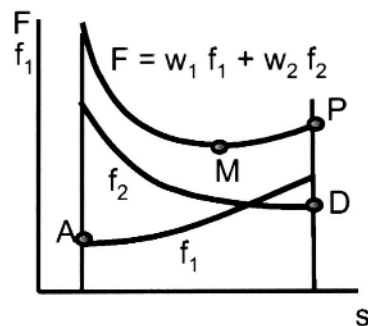One should note another consequence of the non-

Fig. 4 **Non-linear** f_1 **and** f_2

linearity of f_i. The degree of non-linearity in f_1 (or f_2) may be sufficient to make the contours of f_i, curve inside of the $c_i = 0$ boundary, as shown in Fig. 5 for an example of f_1 and c_2. In that situation, by inspection, the minimum of f_i is located at the vertex (South-East vertex in Fig. 5). As to the minimum of F, two possibilities exist. Either the combination of the w_i magnitude with the curvature of f_i is insufficient to curve the contours of F inside of the $c_i = 0$ boundary, in which the previous conclusion about location of P remain qualitatively valid, or it is sufficient to make the F contours curve inside of the $c_i = 0$ boundary. In the latter case, the minimum of F must fall on the vertex just as the minimum of f_1 does in Fig. 5.
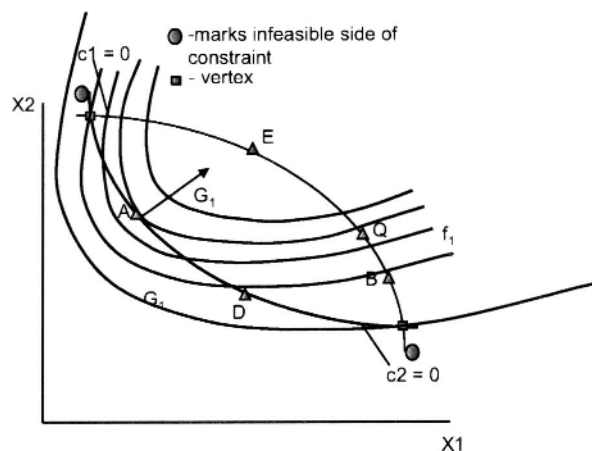

Fig. 5 **Curvature of** f_1 **displacing the function minimum to the vertex**

Implicit in the above discussion is the assumption of convexity of the feasible design space. No general statements can be made for arbitrarily non-convex cases, some of which may be found examined in Ismail-Yahaya and Messac,[2] and Koski[5] and examples provided to show that the Pareto- and non-Pareto frontier may be disjoint when non-convexity
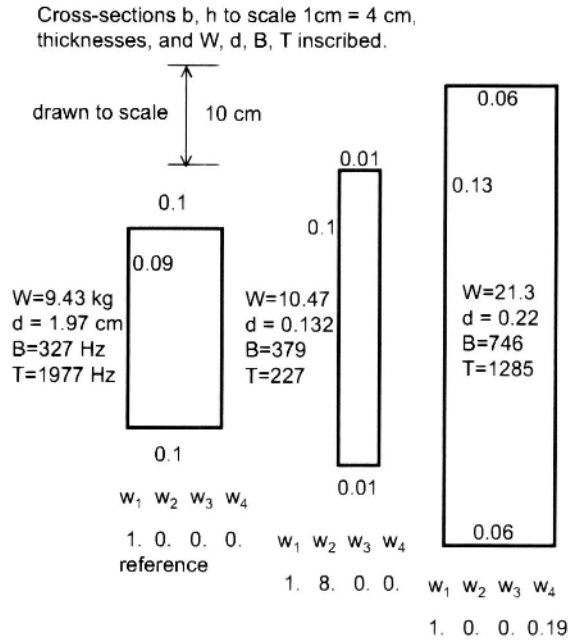
Cross-sections b, h to scale 1cm = 4 cm, thicknesses, and W, d, B, T inscribed.

drawn to scale | 10 cm

0.1

0.09

W=9.43 kg
d = 1.97 cm
B=327 Hz
T=1977 Hz

0.1

w_1 w_2 w_3 w_4

1. 0. 0. 0.
reference

0.01

0.1

W=10.47
d = 0.132
B=379
T=227

0.01

w_1 w_2 w_3 w_4

1. 8. 0. 0.

0.06

0.13

W=21.3
d = 0.22
B=746
T=1285

0.06

w_1 w_2 w_3 w_4

1. 0. 0. 0.19

Fig. 7   Cantilever Beam Results

Fig. 8   Transport Aircraft Wing

$\max(W/W_0)/\min(W/W_0) = 1.94$.

Taking the above example as an indication that the composite objective function approach may have a potential to be effective as a means by which to control the design attributes, attention turns now to a larger test case of a transport aircraft wing.

Larger scale example

Figure 8 displays the finite element model representing the structural box of the wing, and Table 2 provides a description of the FEM. The problem dimensionality in terms of the numbers of the elastic degrees of freedom, constraints, and design variables probably qualifies it as one of the largest cases treated with multi-objective optimization.

The wing cover, rib and spar webs were made of a sheet construction. The model included spar caps, while the rib caps were not modeled. The constraints included equivalent Von Mises stress constraints and tip displacement constraints. The design variables were divided so that 100 of the design variables controlled 2600 quad thickness values, 25 of the design variables controlled 600 rod diameter values and a single design variable controlled the volume change of the wing. The wing volume was changed to preserve the wing span and the depth/chord ratio. Two load conditions were considered: normal lift and engine weight; and landing, half lift and engine weight. The lift was modeled as an equally distributed load over the bottom surface of the wing, engine weight was modeled using point loads and the landing con-
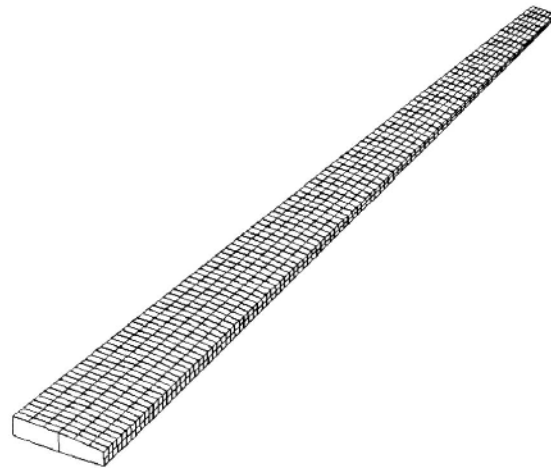
Table 2   Description of the wing test case and its FEM

Parameter	Value
Planform	Trapezoid
Span	70 ft
Chord(Root)	12 ft
Chord(Tip)	3 ft
Depth/Chord	0.2
Sweep Angle	30° aft
Material	Al-alloy
Num. Elements	3008
Num. Nodes	1917
DOF	11400
Design Variables	126
Constraints	24048

dition was modeled as a moment and lifting force distributed over the trailing edge of the wing.

Structural optimization of the aircraft wing was performed using the program GENESIS[8] that integrates optimization and finite element analysis. Three optimization problems were considered: The first problem minimized a combination of the mass and first bending mode frequency; and the second minimized a combination of the mass and the tip rotation of the wing. The third problem considered the mass, first bending mode frequency and the wing internal volume. All design problems had the same design variables, except for the third problem which included the additional design variable that controls the volume.

In all the numerical experiments the optimization was defined as follows, and the f_i functions were

always normalized to eliminate the effect of the magnitude disparity.

Find   Design variables from Table 2

Minimize $F = \sum_i w_i \, f_i$, where $i = 1, ..., N_f$

Satisfy Behavior constraints from Table 2

For the first case, where a combination of the wing mass and first bending mode frequency was considered, the objective function in the wing tests illustrated in Fig. 9

$$F = w_1 \frac{Mass}{Mass_0} + w_2 \frac{Freq}{Freq_0} \qquad (3)$$

where: $Mass$ - wing mass; $Freq$ - first bending mode frequency; $Mass_0$ - mass of the initial design; and $Freq_0$ - first bending mode frequency of the initial design. Both w_1 and w_2 were retained without normalization by w_1 to allow a trade-off study between the mass and frequency (the wing mass was driven up when $w_1 < 0$). Figure 9(a) shows the F variance over a grid of w_1 and w_2, each allowed variability over a fairly broad interval of ± 5 with an increment of 0.5. Of course, $w_1 = w_2 = 0$ is a degenerate case that produced no results; the other degenerate case is the diagonal $w_1 = w_2$). The variance of F is relatively small compared to the variance of the mass and frequency plots (see Figs. 9(b) and 9(c) respectively). The normalized mass and frequency values are shown in Figs. 9(b) and 9(c), using the same grid as shown in Fig. 9(a). These figures show that by manipulating w_1 and w_2 one may create a family of wing designs, bounded by light and high frequency and heavy and low frequency designs. The bounds are quite wide so that the mass varies from 52% to 180% while the frequency changes from 60% to 258% relative to the reference design. The plots also show that there are limits beyond which the attributes of mass and frequency cannot be pushed, regardless of the magnitude of w_1 and w_2. The attributes appear to be slope-discontinuous functions of w_1 and w_2. These discontinuities were generated, as it was to be expected, by changes in the active constraint set.

Further testing included the attributes of mass and tip rotation, using the following objective function

$$F = w_1 \frac{Mass}{Mass_0} + w_2 \frac{Rot}{Rot_0} \qquad (4)$$

where: Rot - tip rotation; and Rot_0 - tip rotation of the initial design. These tests generated results presented in Fig. 10. In general the same trends are present in Fig. 10, as compared to Fig. 9. The
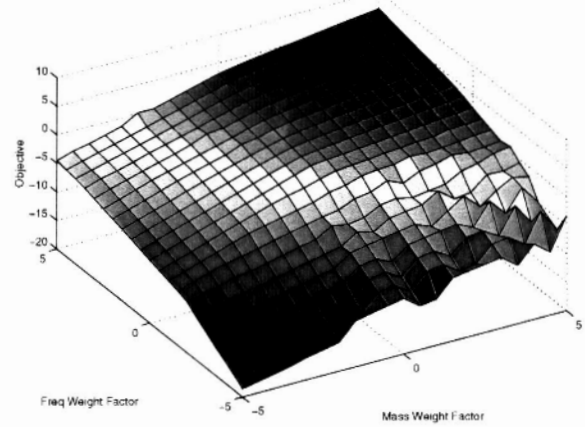
a) Objective Function
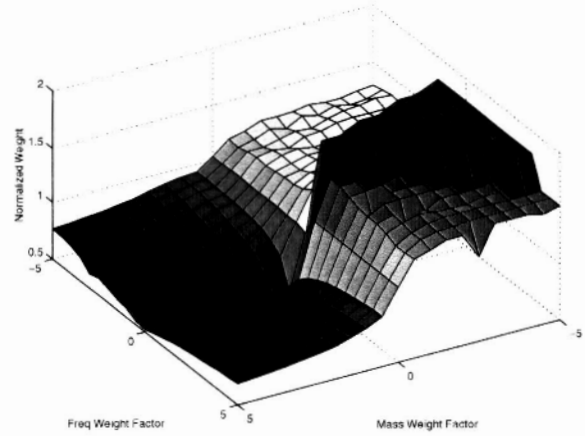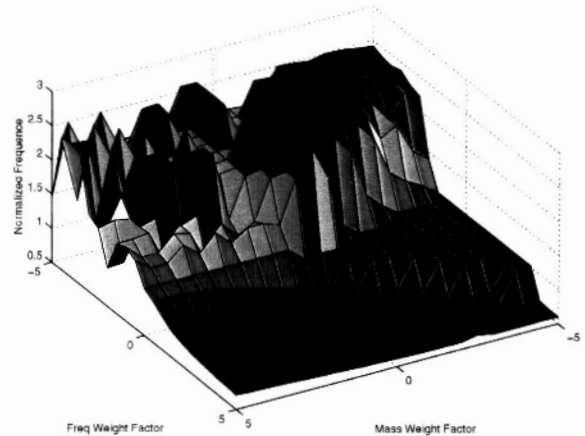
b) Mass Component

c) Frequency Component

Fig. 9 Mass and Frequency Case

variance of F is small compared to that of the mass and tip rotation attributes. Also the variance in F is of a smooth nature, while the mass and tip rotation attributes show variance with a discontinuous

behavior. As before, the attributes vary broadly: 52% to 180% for the mass and 51% to 206% for the tip rotation, relative to the reference design. Again, there are limits beyond which the attributes of mass and frequency cannot be pushed, regardless of the magnitude of w_1 and w_2.

Another feature of the individual attribute surfaces in Figs. 9 and 10 are their stepped structure corresponding to the changes in the critical constraint set and certain amount of noise where, apparently, the optimizer encountered numerical difficulties at the peripheries of the intervals.

The next set of numerical experiments pertained to the objective function extended to include the internal volume of the wing box, an attribute of interest if the wing is used as a fuel tank

$$F = w_1 \frac{Mass}{Mass_0} + w_2 \frac{Freq}{Freq_0} + w_3 \frac{Vol}{Vol_0} \qquad (5)$$

where: Vol - internal volume of the wing; and Vol_0 - internal volume of the initial design. The set of constraints was augmented with the constant ratio of depth/chord.

The optimizations were carried out on a grid in the space of (w_1, w_2, w_3) in which each w_i varied from -5 to +5 with a step size of 0.5. The result was a data base in 3 dimensions (a 3D cloud of points). To visualize the data on 2D scatter plots, a series of cuts were made through the data base and displayed in figures: Fig. 11 - a series of frequency vs. mass plots for 6 values of volume; Fig. 12 - a series of volume vs. frequency plots for 6 values of mass; and Fig. 13 - a series of 6 volume vs. mass plots for 6 values of frequency (all data normalized).

The diagrams show variations of the attributes in quite wide intervals, typically 5 units wide (i.e., 0.5 to 2.5). The shape of the cloud of points may be visualized if one thinks of the series of 6 graphs as snapshots taken while the third attribute advances, e.g., in Fig. 11 the volume advances as indicated by its values inscribed on top of each frame. The cloud of points grows from the single point displayed in Fig. 11(a) to its largest size reached in Fig. 11(f). It may be useful to think of the cloud of points as a two-dimensional analog of the projection of the contour in Fig. 3 on the f_1 and f_2 axis between A and B, and between D and E.

The distribution of points is markedly non-uniform as typical for the composite objective approach[2, 5] and its bandedness is a reflection of the feasible space boundaries that have been previously shown in Figs. 9 and 10 as consisting of curved surfaces and nearly level plateaus. Wherever these plateaus are nearly perpendicular to the attribute
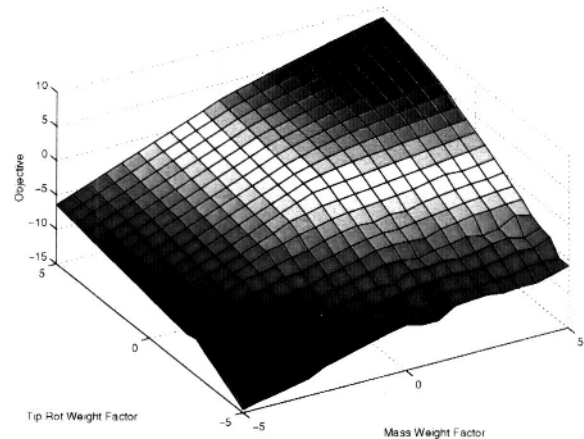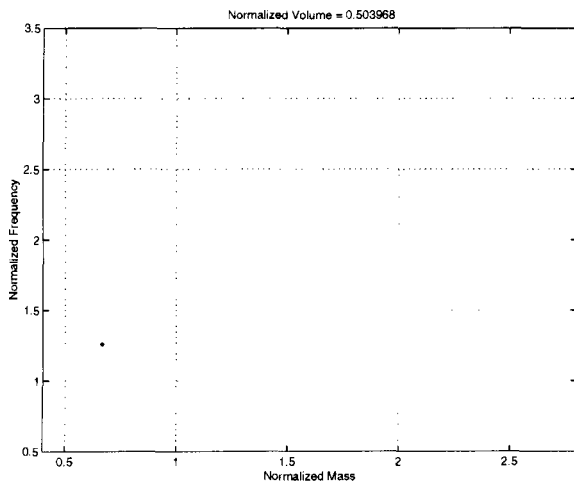


a) Objective Function
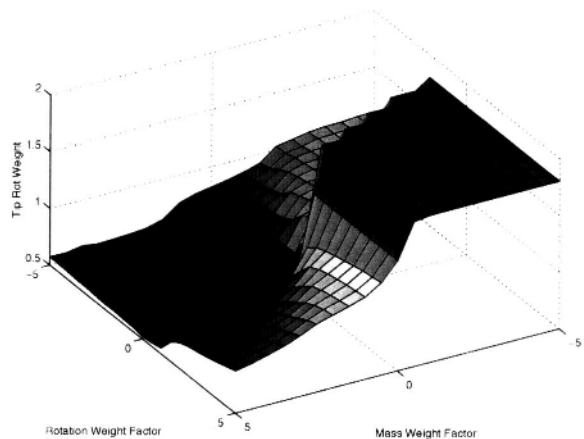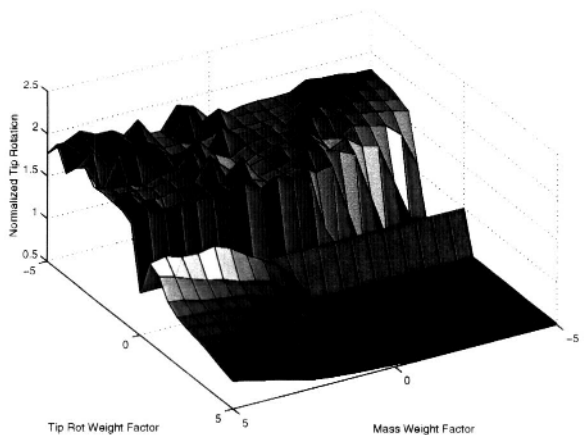
b) Mass Component

c) Tip Rotation Component

Fig. 10   Mass and Tip Rotation Case

plane, their projection appears as a band of points as in Figs. 11–13. The straight vertical lines that bound the clouds of points in Figs. 12(b)–12(f) and 13(b)–13(f) reflect the boundaries of the attribute space.
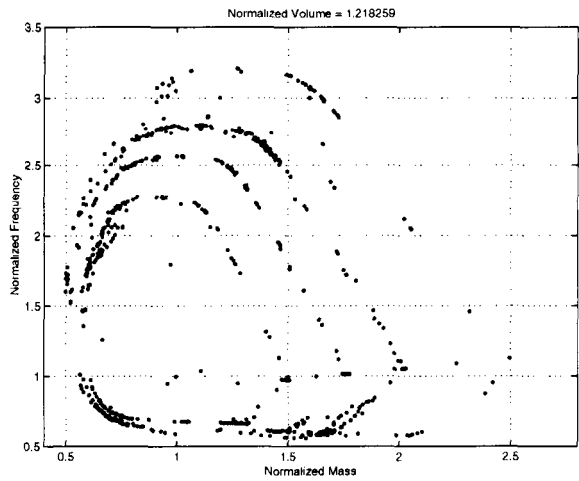
AMERICAN INSTITUTE OF AERONAUTICS AND ASTRONAUTICS

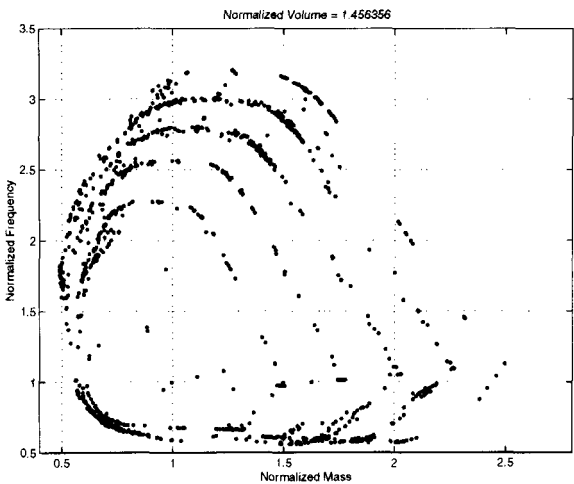**a)** Normalized Volume = 0.503968
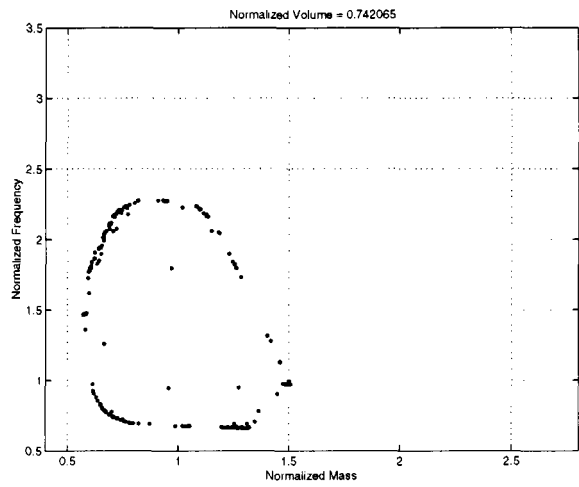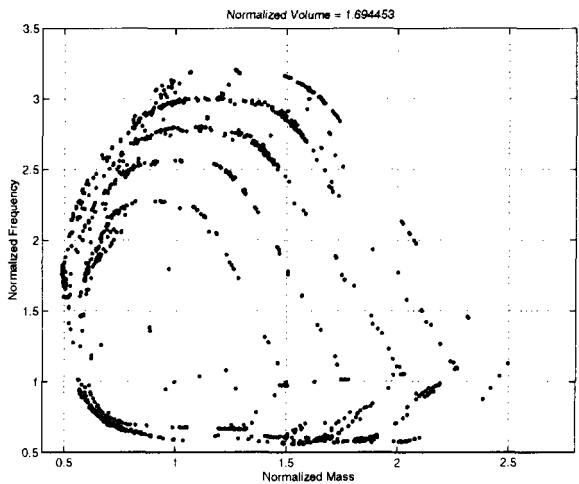

b) Normalized Volume = 0.742065
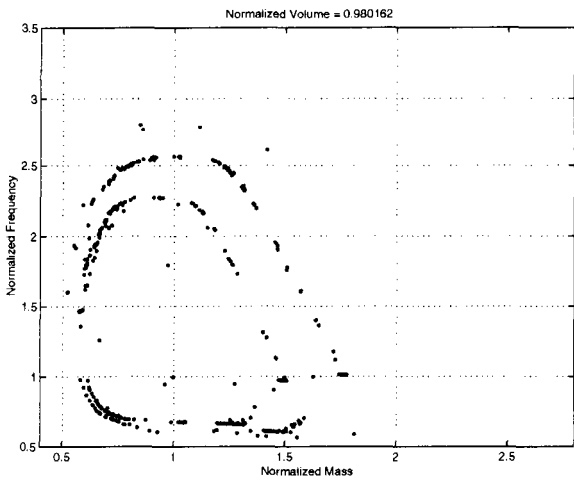
c) Normalized Volume = 0.980162

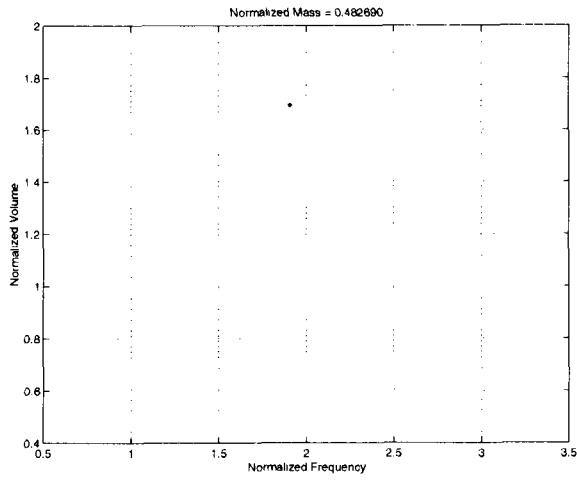**d)** Normalized Volume = 1.218259

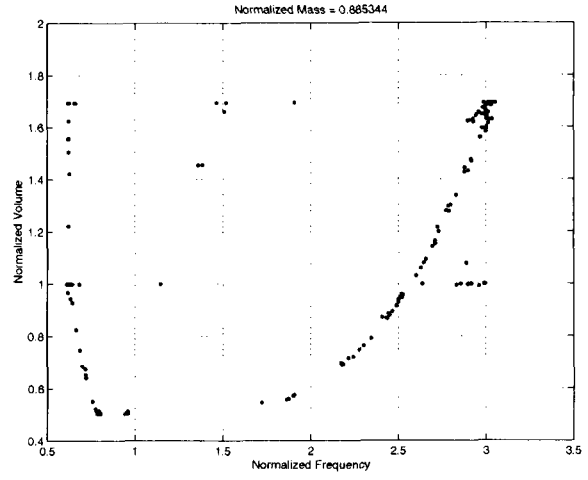
e) Normalized Volume = 1.456356
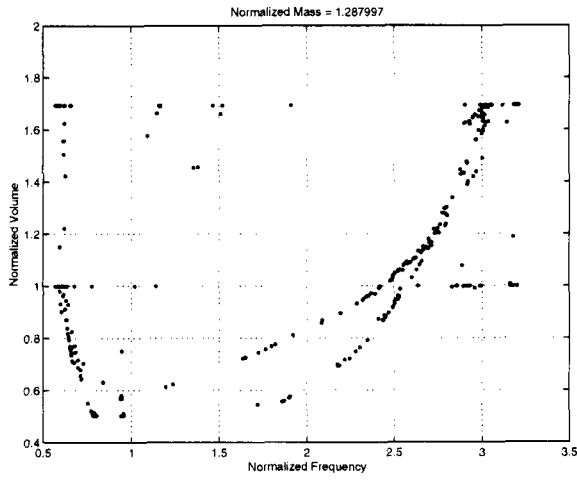

f) Normalized Volume = 1.694453

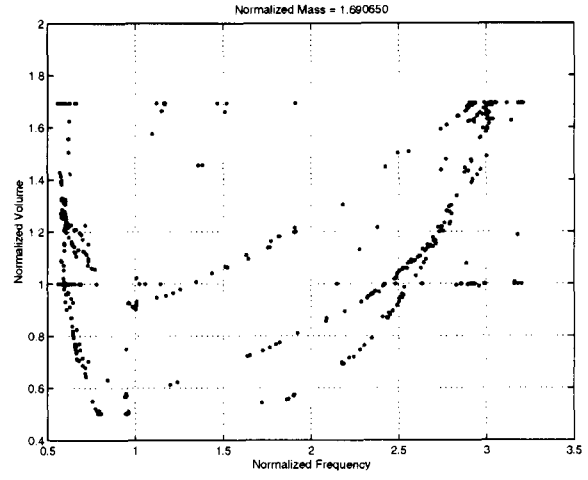**Fig. 11   Mass, Frequency, Volume Case: Normalized Volume**
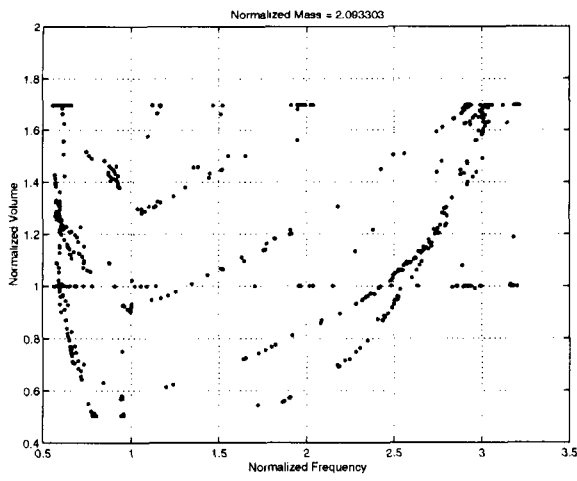
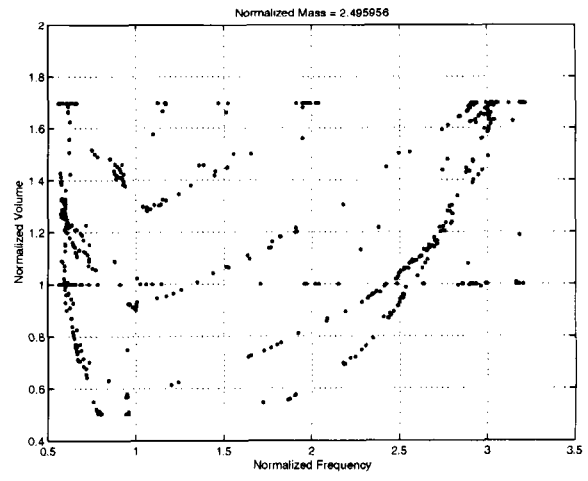a) Normalized Mass = 0.482690

b) Normalized Mass = 0.885344

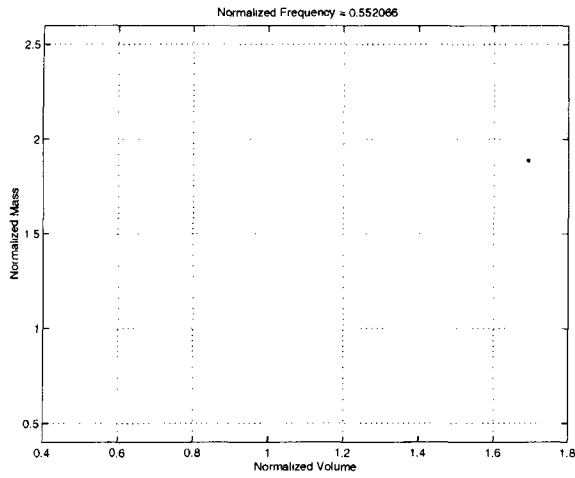c) Normalized Mass = 1.287997

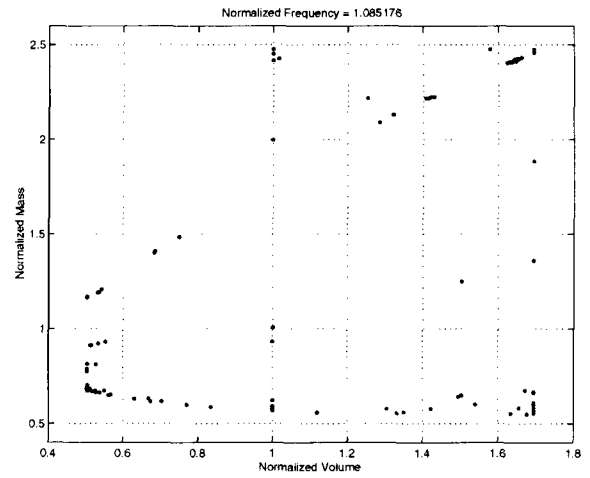d) Normalized Mass = 1.690650

e) Normalized Mass = 2.093303
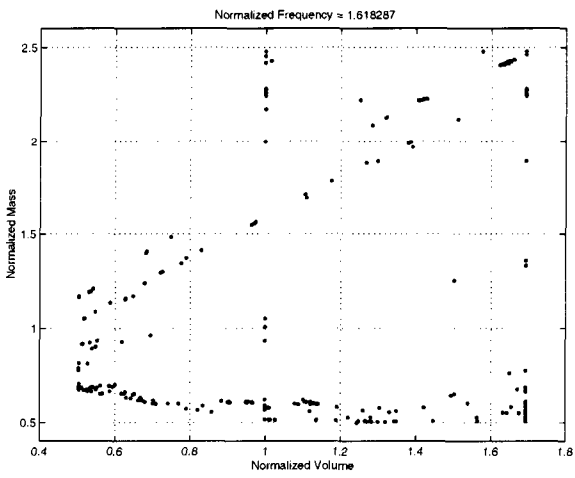
f) Normalized Mass = 2.495956

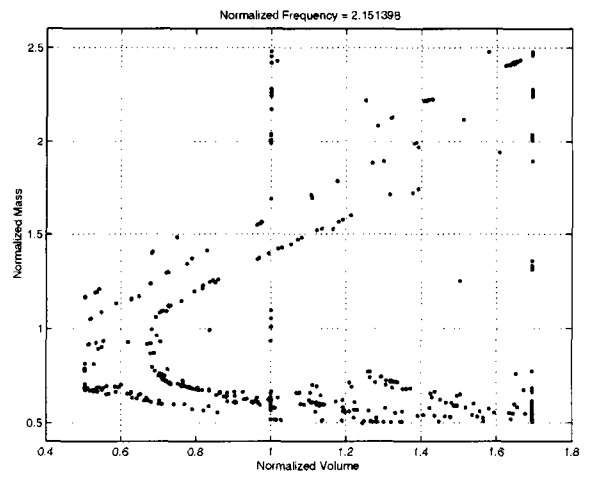Fig. 12   Mass, Frequency, Volume Case: Normalized Mass
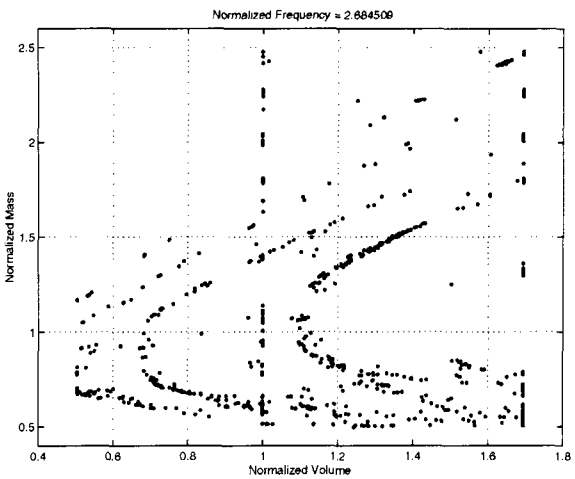
a) Normalized Frequency = 0.552066
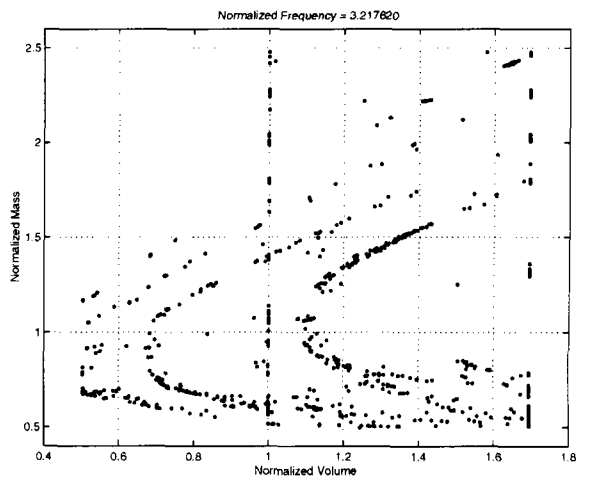
b) Normalized Frequency = 1.085176

c) Normalized Frequency = 1.618287
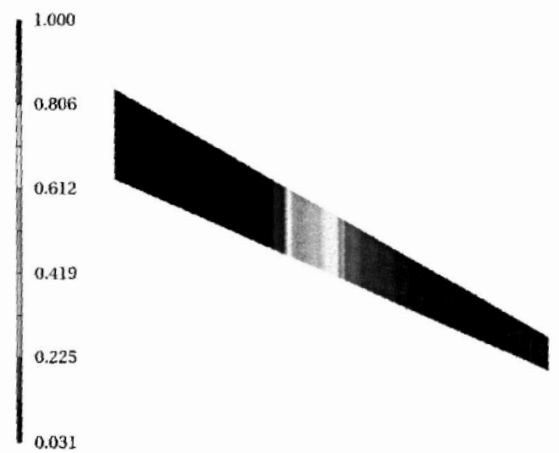
d) Normalized Frequency = 2.151398

e) Normalized Frequency = 2.684509

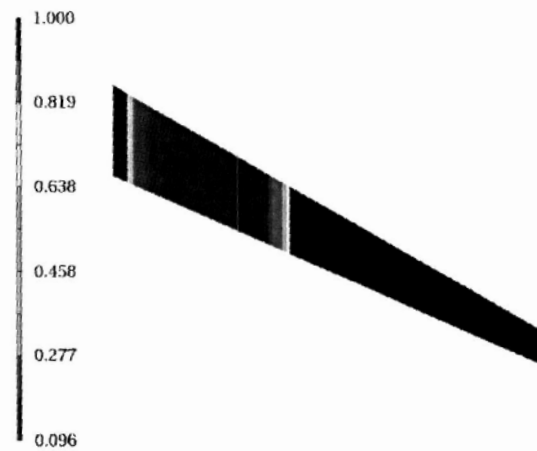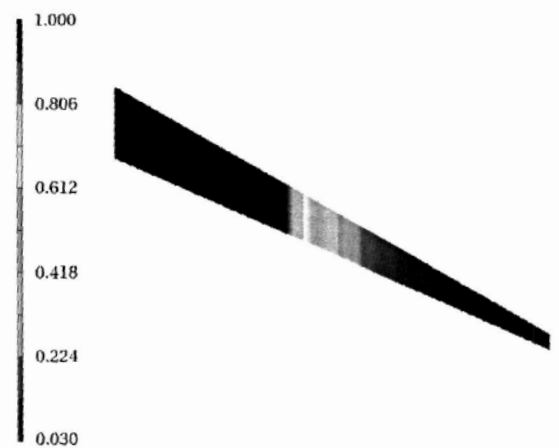f) Normalized Frequency = 3.217620

Fig. 13   Mass, Frequency, Volume Case: Normalized Frequency

a) Norm Vol =1.69, Norm Mass=1.51, Norm Freq=3.16
$w_1 = -1$, $w_2 = -4$, $w_3 = 1$

b) Norm Vol=1.69, Norm Mass=2.00, Norm Freq =0.57
$w_1 = -1$, $w_2 = 5$, $w_3 = -1$

c) Norm Vol=0.89, Norm Mass=1.21, Norm Freq=2.34
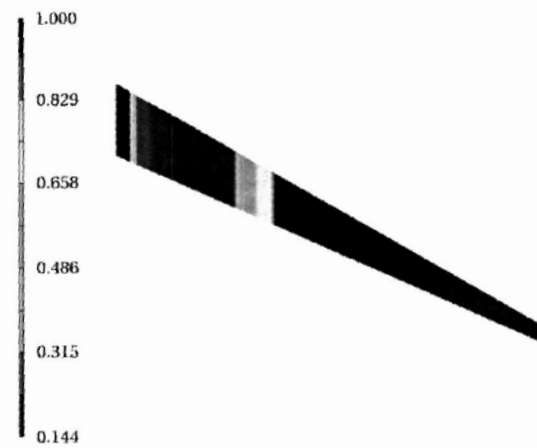$w_1 = -2$, $w_2 = -3$, $w_3 = 4$
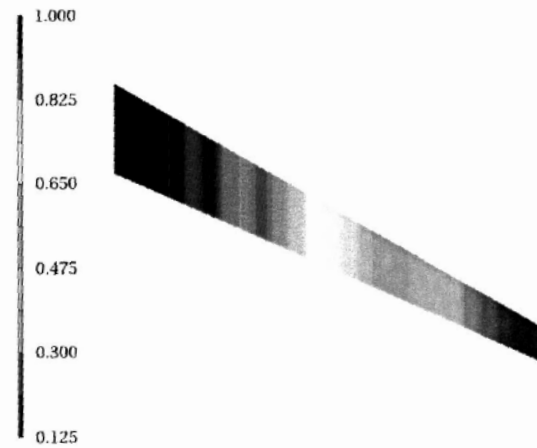
d) Norm Vol=1.69, Norm Mass=0.51, Norm Freq=1.87
$w_1 = 4$, $w_2 = 0$, $w_3 = -4$
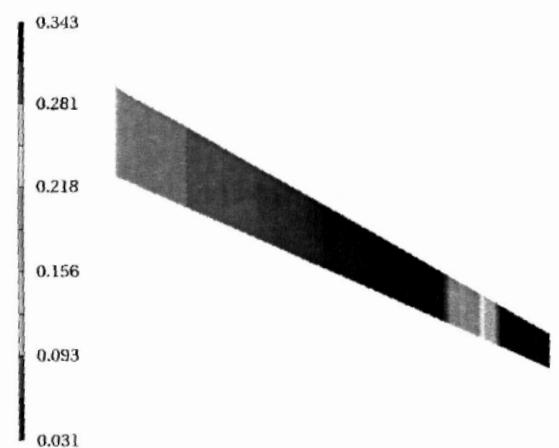
e) Norm Vol=1.69, Norm Mass=0.71, Norm Freq =0.71
$w_1 = 4$, $w_2 = 3$, $w_3 = -3$

f) Norm Vol=1.05, Norm Mass=1.44, Norm Freq=0.62
$w_1 = -5$, $w_2 = 4$, $w_3 = 5$

Fig. 14   Top Cover Thickness Contours

Even though the boundary of the cloud of points is fuzzy as a result of the non-uniform point distribution, the cloud silhouette in Figs. 11–13 appears to the observer as defined fairly clearly owing to the human sense of sight remarkable capability to discern patterns. This adds to the utility of the method especially when used with an aid of a computer monitor in an interactive manner.

Contours of the wing cover sheet thickness plotted in Fig. 14 for six combinations of the attributes and the w-coefficients provide one detailed level example of the diversity of the designs obtained.

The obvious alternative to the composite function approach is to probe for the boundaries of the cloud by optimizing with target values prescribed for the objective. To provide a comparison of this approach with the composite function method, the following optimization was carried out

Find X

Minimize $F = \left(f_1 - f_1^T\right)^2$

Satisfy   Behavior constraints from Table 2
$$\left(f_2 - f_2^T\right) = 0$$
$$\left(f_3 - f_3^T\right) = 0$$

where f_1 is the normalized volume, f_2 is the normalized mass, f_3 is the normalized frequency, and f_1^T, f_2^T, f_3^T are the corresponding target values. The GENESIS objective function history and constraint violation history plots are shown in Fig. 15. It is evident that although the optimizer is able to find a feasible solution very quickly, the convergence is very slow (an arbitrary limit of 100 on the number of iterations was set). In comparison, an equivalent weighted sum approach required less than 10 design iterations for full convergence. There is also a potential for a "no feasible solution" result returned by the optimizer. This possibility must be noted as a demerit of the alternative method because many optimizers return meaningless solutions when unable to converge to a feasible point, so this approach would then have to be executed in a trial-and-error fashion.

Conclusions

The study reported herein led to the following observations:

- Multi-objective optimization based on the simplest technique of the composite objective function was shown by a descriptive geometry argument to be able to return the design points that are in the feasible space or, most often, on
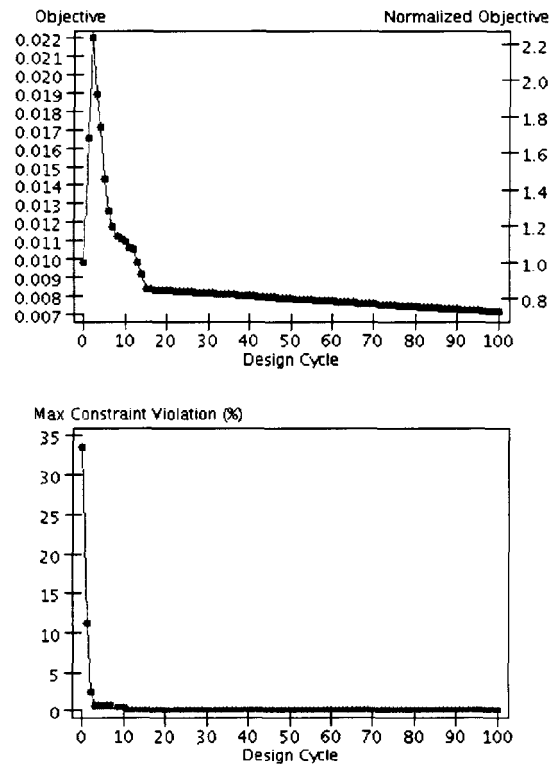

Fig. 15   GENESIS History Data

its boundary when the weight coefficients are varied in magnitude and in sign.

- The magnitudes of individual attributes associated with these points change in a broad range within the domain of the composite function weight coefficients.

- In the w-domain, the individual attributes exhibit slope discontinuities related to the changes in the active constraint set, as well as a certain amount of numerical noise.

- There are limits on individual attributes and their ratios.

- The wing example results show that the attributes of mass, displacement, and vibration trade for each other in very wide ranges. Exploitation of these trade-offs may be useful in a vehicle design, especially if one needs to tune the aeroelastic behavior, or control interaction of the structure with other subsystems.

- Attempt to explore the range of attributes by the target method showed that method as impractical because it may be unable to find a feasible solution for targets beyond reach. In

AMERICAN INSTITUTE OF AERONAUTICS AND ASTRONAUTICS

contrast, making the w-coefficients larger than they need to be is not detrimental in the composite function-based approach.

- On the other hand, if these coefficient ranges are too small, the feasible design will not be explored in full. That calls for judgment in setting these ranges.

- Although parallel computing was not in the scope of this study, it is self-evident that the method is amenable to the use of existing analysis and optimization codes in the manner of a coarse-grained parallelism. In that mode, the time for exploration of the design space may be reduced to the time of a single optimization should a sufficient number of processors be available.

- The limitations on the attributes and their ratios are defined as fuzzy outlines of the clouds of points but the clarity of that definition to the human observer appears to be sufficient as an aid in making design decisions.

Overall, the multi-objective optimization based on the composite objective function technique was found to be a simple and practical tool for exploring the design space for many design attributes simultaneously, including the Pareto- and non-Pareto design points, once the design concept has been decided. It has a potential for providing a fairly clear insight into the design space to determine what is and what is not possible in terms of the design attributes; this information may be particularly useful in guiding specification writing so as to avoid unattainable requirements. It returns a collection of feasible designs from which one can choose, so in this sense it enables a control over the design in a range of alternatives as opposed to a single point optimum design.

References

[1] Stadler, W., *Multicriteria Optimization in Engineering and in the Sciences*, Plenum Press, 3rd ed., 1988.

[2] Ismail-Yahaya, A. and Messac, A., "Effective Generation of the Pareto Frontier: Normalized Normal Constraint Method," *Proceedings of the 43rd AIAA/ASME/ASCE/AHS/ASC Structures, Structural Dynamics, and Materials Conference, Denver, CO*, AIAA-2002-1232, April 22-25 2002.

[3] Messac, A. and Ismail-Yahaya, A., "Required Relationship Between Objective Function and Pareto Frontier Orders: Practical Implications," *AIAA Journal*, Vol. 39, No. 11, Nov. 2001, pp. 2168–2174.

[4] Das, I. and Dennis, J. E., "A Closer Look at Drawbacks of Minimizing Weighted Sum of Objectives For Pareto Set Generation in Multicriteria Optimization Problems," *Structural Optimization*, Vol. 14, 1997, pp. 63–69.

[5] Koski, J., "Multicriteria Truss Optimization," *In Multicriteria Optimization in Engineering and in the Sciences, Plenum Press, 3rd Edition, Stadler (ed.)*, 1988, p. 278.

[6] Belegundu, A. and Chandrupatla, T., *Optimization Concepts and Applications in Engineering*, Prentice Hall, 1999.

[7] Eschenauer, H. A., "Multicriteria Optimization Techniques in Highly Accurate Focusing Systems," *In Multicriteria Optimization in Engineering and in the Sciences, Plenum Press, 3rd Edition, Stadler (ed.)*, 1988, p. 316.

[8] *GENESIS Version 7.0 Users Manual*, Vanderplaats Research and Development, Inc., 2001.